

# Multi-rate real-time model-based parameter estimation and state identification for induction motors

Song Wang<sup>1</sup>, Venkata Dinavahi<sup>2</sup>, Jian Xiao<sup>1</sup>

<sup>1</sup>School of Electrical Engineering, Southwest Jiaotong University, Chengdu 610031, People's Republic of China

<sup>2</sup>Department of Electrical and Computer Engineering, University of Alberta, Edmonton, Canada T6G 2V4

E-mail: songwang@home.swjtu.edu.cn

**Abstract:** This study presents multi-rate parameter and state estimation methods for the induction motor. Based on multi-rate control theory and the extended Kalman filter (EKF) theory, a multi-rate EKF algorithm including input and output algorithms is proposed for load torque estimation in the induction motor. The methods are implemented in real-time on PC-cluster node which acts as the controller for an induction motor experimental set-up. Rotor time constant is a sensitive variable in indirect field-oriented control method. A multi-rate model reference adaptive system (MRAS) is proposed to estimate the rotor time constant in order to guarantee the high-performance control of induction motor. Experimental result verified the effectiveness of the algorithms. Simulations compare the multi-rate EKF algorithm with the traditional single-rate EKF algorithm performance to show improved performance of load torque estimator. The comparison between the traditional MRAS and the multi-rate MRAS shows the superiority of the proposed method, with a satisfactory accuracy.

## 1 Introduction

The induction motor is the most commonly used electric machine in high-performance drive applications. Field-oriented control (FOC) and direct torque control are the main control methods, which require accurate estimation of motor parameters to achieve their control objectives. Although many well-known methods can be used to accurately determine the parameter values under standstill, these parameters may vary during motor operation. Among these parameters, rotor time constant (defined as ratio of rotor inductance to rotor resistance) is the most sensitive variable [1]. Rotor inductance may change because of the flux saturation and rotor resistance varies because of temperature increase. In the FOC, the mismatch of rotor time constant makes the subdivision of stator current into the  $d$ - and  $q$ -axes incorrect which leads to incorrect rotor field angle. Another key to controller design is the knowledge of motor state. In an AC drive system, motor load torque is an important time-varying external disturbance [2]; the variation of load torque should be considered in the design of the speed control system. From the motor equations, the system characteristic is decided by the motor output torque. Therefore the load torque online estimation is essential for motor state observation. Although accurate parameter estimation is the basis of high-performance AC drive, noisy signals affect the estimation convergence, estimation bias and estimated value variance. The parameter mismatch and noisy values could deteriorate the desired control performance [3]. In order to

avoid motor mal-operation, the estimated values of rotor time constant and load torque should be smooth.

In the literature, there are many methods to estimate the motor state and parameter [4–15] include: direct calculation method, model reference adaptive system (MRAS), extended Kalman filter (EKF) and observer-based methods. The EKF algorithm was proposed to handle non-linear problems, this method is based on a stochastic approach and is useful in indirect FOC [12, 13] as shown in Fig. 1a. The EKF method assumes that the measurements of inputs and outputs signals are subjected to white Gaussian noise and tries to estimate/predict the state variables  $\hat{x}_k$  to minimise the noise effect. The MRAS system consists of three parts: a reference model, an adjustable model and an adaptive mechanism. The basic structure of MRAS is shown in Fig. 1b. The quantity calculated from the adjustable model  $\hat{x}$  is compared to the measured value  $x^*$  from the reference model; the error  $e$  between the states of the two models is then used to drive the adaptive mechanism to estimate the quantity's value. EKF and MRAS are the commonly used methods because of their ability to effectively eliminate random noise, and relatively simple implementation requirement. An EKF estimation method that is effective over a wide velocity is presented in [2], and Pea *et al.* [8] present an MRAS method which estimates rotor position and speed from machine currents. However, these methods are based on the motor mathematical model, and utilise a single-rate implementation, that is, the system's sampler and hold work with the same sampling periods. This paper present

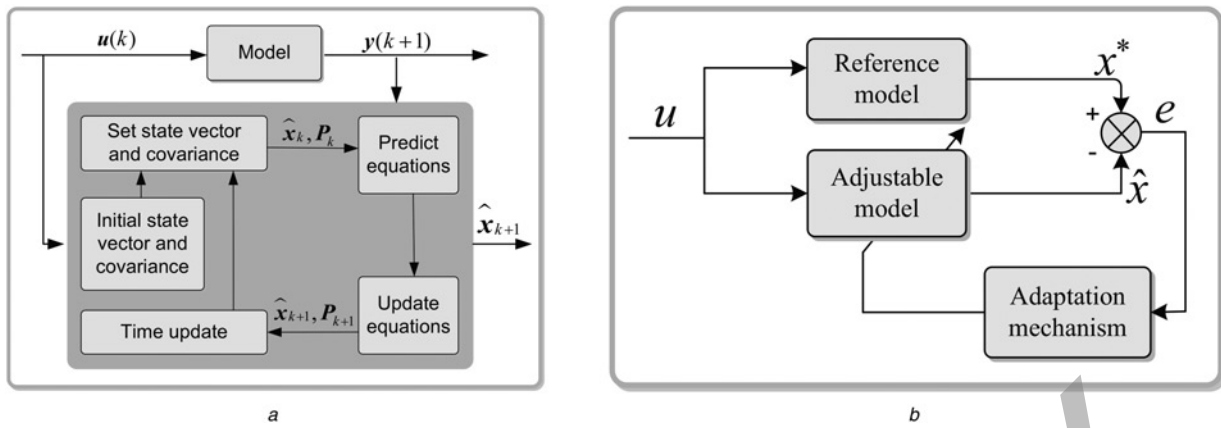


**Fig. 1** Structure of model based parameter estimation and state identification system  
 a Structure of extended Kalman filter system  
 b Structure of model reference adaptive system

multi-rate EKF and MRAS method and implemented the method in real-time on PC cluster node. EKF and MRAS are chosen for their universality.

Digital control systems are hybrid systems, involving both continuous-time and discrete-time signals. In sampled-data control systems, it is usually assumed that all the signals in the system are sampled simultaneously with a single rate to simplify the analysis. With the increase of the controlled object size and complexity, the rate of change of different signals varies greatly; therefore adopting a single sampling rate everywhere is unrealistic. A system whose sampler and hold work with different sampling periods is known as a multi-rate digital control system [16]. Other reasons such as large differences between the time constants of the various feedback loops of the plant, and between the time needed to measure the respective variables, also make multi-rate sampling unavoidable. The multi-rate sample-data control system has been the topic of interest for several years. The main research directions of this technique are: intersample behaviour [17, 18], pole assignment [19], lifting approach and  $H_2$ -optimal and  $H_\infty$  design [20, 21]. The advantages of multi-rate control include improved system performance, less cost, improved controllability and observability. Multi-rate control can also realise many functions, which single-rate control cannot, such as improved system gain margin, strong stabilisation, simultaneous stabilisation, decentralised control and robust control [22–24].

This paper proposes multi-rate real-time model-based parameter estimation algorithms for induction motors. The proposed multi-rate EKF method combines multi-rate control and EKF to estimate motor load torque, introducing both input and output algorithms. The method achieves joint speed and load torque estimation, and is implemented in real-time on PC-cluster node which acts as the controller for an induction motor experimental set-up. A multi-rate MRAS method is proposed to estimate rotor time constant. The paper is organised as follows: Section 2 presents multi-rate parameter estimation methods; motor model, multi-rate EKF and multi-rate MRAS algorithms are explained. Experimental results and comparison between single-rate and multi-rate implementations are provided in Section 3. Conclusions appear in Section 4.

## 2 Multi-rate parameter estimation methods

### 2.1 Induction machine model

The induction motor model can be described in  $dq$  frame as fourth-order state equation [25]. Assuming that the induction motor rotor speed and load torque to be the unknown state variables. Combining induction motor motion and torque equations, a sixth-order state equation is constituted in the two-phase  $dq$  frame as below

$$\begin{cases} \dot{x} = Ax + Bu + w \\ y = Cx + v \end{cases} \quad (1)$$

where the state vector is

$$x = [i_{sd} \quad i_{sq} \quad \lambda_{rd} \quad \lambda_{rq} \quad \omega_r \quad T_l]^T \quad (2)$$

with stator currents  $i_{sd}, i_{sq}$ ; rotor fluxes  $\lambda_{rd}, \lambda_{rq}$ ; rotor speed  $\omega_r$ ; and load torque  $T_l$ . The input vector stator voltage  $u = [u_{sd} \quad u_{sq}]^T$  and the output vector  $y = [i_{sd} \quad i_{sq}]^T$ .  $w(6 \times 1)$  and  $v(2 \times 1)$  are the process and observation noises, which are both assumed to be zero mean multivariate Gaussian noises with covariance  $Q(6 \times 6)$  and  $R(2 \times 2)$ , respectively.

The coefficient matrices in (1) are given as

$$A(6 \times 6) = \begin{bmatrix} -\xi & 0 & \frac{\eta}{\tau_r} & \eta\omega_r & 0 & 0 \\ 0 & -\xi & -\eta\omega_r & \frac{\eta}{\tau_r} & 0 & 0 \\ \frac{L_m}{\tau_r} & 0 & -\frac{1}{\tau_r} & -\omega_r & 0 & 0 \\ 0 & \frac{L_m}{\tau_r} & \omega_r & -\frac{1}{\tau_r} & 0 & 0 \\ -\frac{3n_p L_m}{JL_r} \lambda_{rq} & \frac{3n_p L_m}{JL_r} \lambda_{rd} & 0 & 0 & 0 & -\frac{1}{J} \\ 0 & 0 & 0 & 0 & 0 & 0 \end{bmatrix} \quad (3)$$

$$\mathbf{B}(6 \times 2) = \begin{bmatrix} \frac{1}{\sigma L_s} & 0 & 0 & 0 & 0 & 0 \\ 0 & \frac{1}{\sigma L_s} & 0 & 0 & 0 & 0 \end{bmatrix}^T \quad (4)$$

$$\mathbf{C}(2 \times 6) = \begin{bmatrix} 1 & 0 & 0 & 0 & 0 & 0 \\ 0 & 1 & 0 & 0 & 0 & 0 \end{bmatrix} \quad (5)$$

where

$$\xi = \frac{R_s}{\sigma L_s} + \frac{1 - \sigma}{\sigma \tau_r}, \quad \eta = \frac{L_m}{L_s L_r - L_m^2},$$

$$\sigma = 1 - \frac{L_m^2}{L_s L_r}, \quad \tau_r = \frac{L_r}{R_r}$$

where  $R_s$ ,  $R_r$ ,  $L_s$ ,  $L_r$  and  $L_m$  are the stator resistance, rotor resistance, stator inductance, rotor inductance and magnetising inductance, respectively.

Assume  $\omega_r$  and  $T_l$  are kept constant during sampling period  $T$ . Using the lifting technique, the following linear time-invariant state-space description of the induction motor in discrete-time can be formulated

$$\begin{cases} \mathbf{x}(k+1) = \mathbf{A}(k)\mathbf{x}(k) + \mathbf{B}(k)\mathbf{u}(k) + \mathbf{w}(k) \\ \mathbf{y}(k) = \mathbf{C}\mathbf{x}(k) + \mathbf{v}(k) \end{cases} \quad (6)$$

In the above equation, the coefficient matrices  $\mathbf{A}(k)(6 \times 6)$  and  $\mathbf{B}(k)(6 \times 2)$  are given as (see (7))

$$\mathbf{B}(k) = \begin{bmatrix} \frac{T}{\sigma L_s} & 0 & 0 & 0 & 0 & 0 \\ 0 & \frac{T}{\sigma L_s} & 0 & 0 & 0 & 0 \end{bmatrix}^T \quad (8)$$

## 2.2 Multi-rate sampled-data control system

Consider the multi-rate sampled-data control system shown in Fig. 2, where  $P_c$  is the  $m$ -input  $p$ -output linear continuous plant;  $C_d$  is the multi-rate digital controller;  $H$  is the multi-rate zero-order hold; and  $S$  is the multi-rate sampler.  $r_c$ ,  $y$  and  $e = r_c - y$  are the reference input, the output and the tracking error of the system, respectively.

Assume that the sampling periods for the input  $u$  and the error  $e$  are, respectively, defined as:  $T_{ui} = q_{ui}T$ ,  $i = 1, 2, \dots, m$ ;  $T_{ei} = q_{ei}T$ ,  $i = 1, 2, \dots, p$ , where all the  $q_{ui}$ 's and  $q_{ei}$ 's are positive integers and  $T$  is the base-rate sampling period. Thus, all sampling periods in the overall system are integer

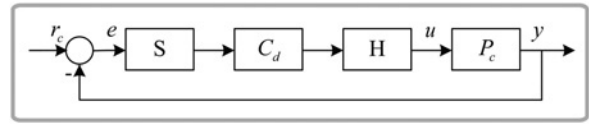


Fig. 2 Multi-rate sampled-data control system

multiples of the base-rate period  $T$ , and all are synchronised to the 'frame period'  $T_f = qT$ ;  $q$  is the least common multiple of  $q_{ui}$  and  $q_{ei}$ . The frame period and sampling multiplicity are generalised definitions for all multi-rate control and estimation systems.

## 2.3 Multi-rate EKF-based load torque estimation

In order to present an exhaustive view of multi-rate EKF method, in this section two multi-rate algorithms are proposed for load torque estimation: input multi-rate EKF algorithm and output multi-rate EKF algorithm; the focus of the estimation method is on the mechanical variables  $\omega_r$  and  $T_l$ . However, for ease of understanding, we introduce the single-rate EKF algorithm first.

**2.3.1 Single-rate EKF algorithm:** The EKF is the extension of conventional Kalman filter which can handle non-linear systems, that is, the state transition and observation models can be non-linear functions of the state. The algorithm classifies into three strategies according to the relationship of sampling periods of input and output vector. Single-rate EKF is the traditional EKF algorithm where the sampling period of input equals the sampling period of the output. The EKF algorithm mainly contains a 'predict' stage and an 'update' stage. Further details of the single-rate EKF algorithm can be found in [26].

**2.3.2 Input multi-rate EKF algorithm:** The controlled object is described by state (1), where the sampling period of output vector  $\mathbf{y}$  is  $T_o$ , the sampling period of input vector  $\mathbf{x}$  is  $T_i$ ;  $T_i < T_o$ , assume  $T_o = NT_i$ ,  $N = 1, 2, \dots$ , that is, when output signal is sampled one time, the input signal is sampled  $N$  times.  $N$  is the sampling multiplicity.

Defining the input extended vector

$$\mathbf{u}_i(k)(2N \times 1) = [\mathbf{u}(k) \quad \mathbf{u}(k+1) \quad \dots \quad \mathbf{u}(k+N-1)]^T \quad (9)$$

and its extended coefficient matrix

$$\mathbf{B}_i(6 \times 2N) = [\mathbf{A}^{N-1}\mathbf{B} \quad \mathbf{A}^{N-2}\mathbf{B} \quad \dots \quad \mathbf{B}] \quad (10)$$

$$\mathbf{A}(k) = \begin{bmatrix} 1 - \xi T & 0 & T \frac{\eta}{\tau_r} & T \eta \omega_r & T \eta \lambda_{rq} & 0 \\ 0 & 1 - T \xi & -T \eta \omega_r & T \frac{\eta}{\tau_r} & T \eta \lambda_{rd} & 0 \\ T \frac{L_m}{\tau_r} & 0 & 1 - T \frac{1}{\tau_r} & -T \omega_r & -T \lambda_{rq} & 0 \\ 0 & T \frac{L_m}{\tau_r} & T \omega_r & 1 - T \frac{1}{\tau_r} & -T \lambda_{rd} & 0 \\ -T \frac{3n_p L_m}{J L_r} \lambda_{rq} & T \frac{3n_p L_m}{J L_r} \lambda_{rd} & 0 & 0 & 1 & -\frac{T}{J} \\ 0 & 0 & 0 & 0 & 0 & 1 \end{bmatrix} \quad (7)$$

Defining the extended process noise vector  $w_i(6N \times 1)$  and its coefficient matrix  $B_{iw}(6 \times 6N)$ , as given below

$$w_i(k) = [w(k) \quad w(k+1) \quad \dots \quad w(k+N-1)]^T \quad (11)$$

$$B_{iw} = [A^{N-1}B_w \quad A^{N-2}B_w \quad \dots \quad B_w] \quad (12)$$

where  $B_w(6 \times 6)$  is the coefficient matrix of  $w$ . The discretised state-space model is derived by successive iteration

$$\begin{cases} x(kT_o + NT_i) = A^N x(kT_o) + B_i u_i(kT_o) + B_{iw} w_i(kT_o) \\ y(kT_o) = Cx(kT_o) + v(kT_o) \end{cases} \quad (13)$$

Using the simplifying assumption:  $kT_o + NT_i = (k+1)T_o \sim k+1$ , and substituting extended vectors  $u_i(k)$ ,  $B_i$ ,  $w_i(k)$  and  $B_{iw}$  into the EKF algorithm Fig. 3, the derived motor state estimation recursive algorithm based on input multi-rate EKF algorithm is as follows:

Predict equations:

- $\tilde{x}(k+N) = A^N x(k) + B_i u_i(k)$
- $P_i(k+N|k) = F^N P_i(k|k)(F^N)^T + B_{iw} Q_i (B_{iw})^T$

where the function  $F(6 \times 6)$  can be used to compute the predicted state from the previous estimate: (see (14))

Update equations:

- $K_i(k+N) = P_i(k+N|k)C^T [CP_i(k+N|k)C^T + R_i(k+N)]^{-1}$
- $\hat{x}(k+N|k+N) = \tilde{x}(k+N|k) + K_i(k+N)[y(k+N) - C\tilde{x}(k+N|k)]$
- $P_i(k+N|k+N) = P_i(k+N|k) - P_i(k+N|k)K_i(k+N)C$

$Q_i$  and  $R_i$  are the covariance matrices of process and observation noise, respectively, with  $Q_i = E(w_i w_i^T)$ , and  $R_i = E(v v^T)$ . Fig. 3 shows the flowchart of input multi-rate EKF estimator.

**2.3.3 Output multi-rate EKF algorithm:** The controlled object is the discretised state-space model whose sampling period is  $T_o$ . In contrast to the input algorithm, in the output multi-rate algorithm  $T_i > T_o$ , where  $T_i = NT_o$ ,  $N=1, 2, \dots$ , that is, when the input signal is sampled one time, the output signal is sampled  $N$  times. In period  $T_o$ , the input  $u_k$  is kept constant.

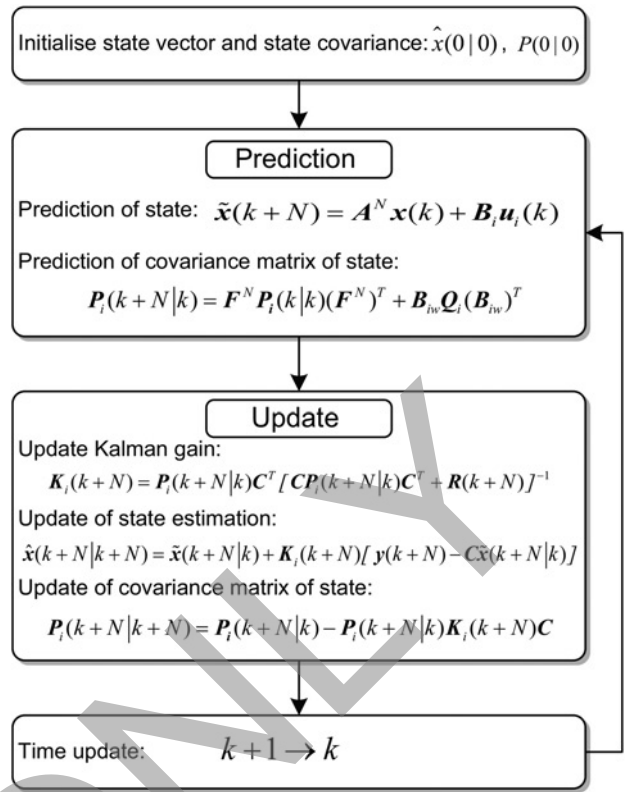


Fig. 3 Flowchart of input multi-rate EKF estimator

Defining the output extended vector as

$$y_o(k)(2N \times 1) = [y(k-N+1) \quad y(k-N+2) \quad \dots \quad y(k)]^T \quad (15)$$

and the input extended vector as

$$u_o(k)(2N \times 1) = [u(k-N+1) \quad u(k-N+2) \quad \dots \quad u(k)]^T \quad (16)$$

the output equation is transformed as

$$y(k-N+1) = Cx(k-N+1) + v(k-N+1) \quad (17)$$

$$F(k) = \left. \frac{\partial f[x(k), k]}{\partial x} \right|_{x(k)=\hat{x}(k)} = \begin{bmatrix} 1 - \xi T & 0 & \frac{\eta}{\tau_r} T & \eta T \hat{\omega}_r(k) & \eta T \hat{\lambda}_{rq}(k) & 0 \\ 0 & 1 - \xi T & -\eta T \hat{\omega}_r(k) & \frac{\eta}{\tau_r} T & -\eta T \hat{\lambda}_{rd}(k) & 0 \\ \frac{L_m}{\tau_r} T & 0 & 1 - \frac{1}{\tau_r} T & -T \hat{\omega}_r(k) & -T \hat{\lambda}_{rq}(k) & 0 \\ 0 & \frac{L_m}{\tau_r} T & T \hat{\omega}_r(k) & 1 - \frac{1}{\tau_r} T & T \hat{\lambda}_{rd}(k) & 0 \\ -T \frac{3npL_m}{JL_r} \hat{\lambda}_{rq}(k) & T \frac{3npL_m}{JL_r} \hat{\lambda}_{rd}(k) & 0 & 0 & 1 & -\frac{T}{J} \\ 0 & 0 & 0 & 0 & 0 & 1 \end{bmatrix} \quad (14)$$

Substituting (6) into (17),  $\mathbf{y}(k-N+1)$  is derived as

$$\begin{aligned} \mathbf{y}(k-N+1) &= \mathbf{C}\mathbf{A}^{-N+1}\mathbf{x}(k) + \mathbf{v}(k-N+1) \\ &\quad - \mathbf{C}\mathbf{A}^{-1}\mathbf{B}\mathbf{u}(k-N+1) \\ &\quad - \mathbf{C}\mathbf{A}^{-2}\mathbf{B}\mathbf{u}(k-N+2) \\ &\quad - \dots - \mathbf{C}\mathbf{A}^{-N+1}\mathbf{B}\mathbf{u}(k-1) \\ &\quad - \mathbf{C}\mathbf{A}^{-1}\mathbf{B}_\omega\omega(k-N+1) \\ &\quad - \mathbf{C}\mathbf{A}^{-2}\mathbf{B}_\omega\omega(k-N+2) \\ &\quad - \dots - \mathbf{C}\mathbf{A}^{-N+1}\mathbf{B}_\omega\omega(k-1) \end{aligned} \quad (18)$$

Other output extended vectors  $\mathbf{y}(k-N+2), \dots, \mathbf{y}(k)$  can also be derived using the same method. Then the output extended vector  $\mathbf{y}_o(k)$  is derived. The coefficient matrices are given as follows

$$\mathbf{C}_o(2N \times 6) = [\mathbf{C}\mathbf{A}^{-N+1} \quad \mathbf{C}\mathbf{A}^{-N+2} \quad \dots \quad \mathbf{C}\mathbf{A}^{-1} \quad \mathbf{C}]^T \quad (19)$$

$$\mathbf{D}_o(2N \times 2N) = \begin{bmatrix} -\mathbf{C}\mathbf{A}^{-1}\mathbf{B} & \dots & -\mathbf{C}\mathbf{A}^{-N+1}\mathbf{B} & 0 \\ \vdots & \vdots & \vdots & \vdots \\ 0 & \dots & -\mathbf{C}\mathbf{A}^{-1}\mathbf{B} & 0 \\ 0 & \dots & 0 & 0 \end{bmatrix} \quad (20)$$

Process and observation noises are  $\mathbf{w}_o(k)$  and  $\mathbf{v}_o(k)$ . Replacing  $\mathbf{y}$  by  $\mathbf{w}$  and  $\mathbf{v}$  in  $\mathbf{y}_o(k)$ , the  $\mathbf{w}_o(k)$  and  $\mathbf{v}_o(k)$  are derived. Replacing the  $\mathbf{B}$  by  $\mathbf{B}_w$  in  $\mathbf{D}_o$ , the process noise extended coefficient matrix  $\mathbf{H}_o(2N \times 6N)$  is derived, where  $\mathbf{B}_w$  is the process noise coefficient matrix

$$\mathbf{w}_o(k)(6N \times 1) = [\mathbf{w}(k-N+1) \quad \mathbf{w}(k-N+2) \quad \dots \quad \mathbf{w}(k)]^T \quad (21)$$

$$\mathbf{v}_o(k)(2N \times 1) = [\mathbf{v}(k-N+1) \quad \mathbf{v}(k-N+2) \quad \dots \quad \mathbf{v}(k)]^T \quad (22)$$

For an arbitrary  $N$ , the output equation is given as

$$\mathbf{y}_o(k) = \mathbf{C}_o\mathbf{x}(k) + \mathbf{D}_o\mathbf{u}_o(k) + \mathbf{H}_o\mathbf{w}_o(k) + \mathbf{v}_o(k) \quad (23)$$

As shown in (23), multi-rate control brings some additional matrices; these matrices require more compute capacity. However, with the development of computer science, the processor could handle these additional computation easily.

The output multi-rate EKF recursive algorithm is as follows:

Predict equations:

- $\hat{\mathbf{x}}(k+N) = \mathbf{A}^N\mathbf{x}(k) + \mathbf{B}_i\mathbf{u}(k)$
- $\mathbf{P}_o(k+N/k) = \mathbf{F}^N\mathbf{P}_o(k/k)(\mathbf{F}^N)^T + \mathbf{B}_{ow}\mathbf{Q}_o(k)(\mathbf{B}_{ow})^T$

Update equations:

- $\mathbf{K}_o(k+N) = \mathbf{P}_o(k+N/k)\mathbf{C}_o^T * [\mathbf{C}_o\mathbf{P}_o(k+N/k)\mathbf{C}_o^T + \mathbf{R}_o(k) + \mathbf{H}_o\mathbf{Q}_o(k)(\mathbf{H}_o)^T]^{-1}$
- $\hat{\mathbf{x}}(k+N|k+N) = \hat{\mathbf{x}}(k+N|k) + \mathbf{K}_o(k+N)[\mathbf{y}_o(k+N) - \mathbf{C}_o\hat{\mathbf{x}}(k+N|k) - \mathbf{D}_o\mathbf{u}_o(k+N)]$

- $\mathbf{P}_o(k+N/k+N) = \mathbf{P}_o(k+N/k) - \mathbf{P}_o(k+N/k)\mathbf{K}_o(k+N)\mathbf{C}_o$

where  $\mathbf{Q}_o$  and  $\mathbf{R}_o$  are the covariance matrices of process and observation noise, respectively,  $\mathbf{Q}_o = E(\mathbf{w}_o\mathbf{w}_o^T)$  and  $\mathbf{R}_o = E(\mathbf{v}_o\mathbf{v}_o^T)$ . Single-rate EKF is a special case of multi-rate EKF algorithm, when sampling multiplicity  $N=1$ .

#### 2.4 Multi-rate MRAS-based rotor time constant estimation

The magnetising current is calculated from the adjustable model and compared to the value from the reference model, to obtain the error which is used to drive the adaptive mechanism to estimate the rotor time constant. Defining magnetising current as

$$i_{dmr} = \frac{\lambda_{dr}}{L_m}, \quad i_{qmr} = \frac{\lambda_{qr}}{L_m} \quad (24)$$

and derived from motor model (1)

$$\begin{cases} \frac{di_{ds}}{dt} = \frac{L_m}{\sigma L_s L_r} \left( \frac{1}{\tau_r} \lambda_{dr} + \omega_r \lambda_{qr} - \frac{L_m}{\tau_r} i_{ds} \right) \\ \quad - \frac{r_s}{\sigma L_s} i_{ds} + \frac{1}{\sigma L_s} v_{ds} \\ \frac{di_{qs}}{dt} = \frac{L_m}{\sigma L_s L_r} \left( \frac{1}{\tau_r} \lambda_{qr} - \omega_r \lambda_{dr} - \frac{L_m}{\tau_r} i_{qs} \right) \\ \quad - \frac{r_s}{\sigma L_s} i_{qs} + \frac{1}{\sigma L_s} v_{qs} \end{cases} \quad (25)$$

substituting  $\lambda_r$  defined in motor model (1) into (25), the following equations can be obtained

$$\begin{cases} \frac{di_{ds}}{dt} = \frac{L_m}{\sigma L_s L_r} \left( -\frac{d\lambda_{dr}}{dt} \right) - \frac{r_s}{\sigma L_s} i_{ds} + \frac{1}{\sigma L_s} v_{ds} \\ \frac{di_{qs}}{dt} = \frac{L_m}{\sigma L_s L_r} \left( -\frac{d\lambda_{qr}}{dt} \right) - \frac{r_s}{\sigma L_s} i_{qs} + \frac{1}{\sigma L_s} v_{qs} \end{cases} \quad (26)$$

The reference model uses the voltage model derived from (24, 26)

$$\frac{d}{dt} \begin{bmatrix} i_{dmr} \\ i_{qmr} \end{bmatrix} = \frac{L_r}{L_m^2} \begin{bmatrix} v_{ds} \\ v_{qs} \end{bmatrix} - \begin{bmatrix} \left( r_s i_{ds} + \sigma L_s \frac{di_{ds}}{dt} \right) \\ \left( r_s i_{qs} + \sigma L_s \frac{di_{qs}}{dt} \right) \end{bmatrix} \quad (27)$$

The parallel adjustable model uses the current model

$$\frac{d}{dt} \begin{bmatrix} \hat{i}_{dmr} \\ \hat{i}_{qmr} \end{bmatrix} = \begin{bmatrix} -\frac{1}{\hat{\tau}_r} & -\omega_r \\ \omega_r & -\frac{1}{\hat{\tau}_r} \end{bmatrix} \begin{bmatrix} \hat{i}_{dmr} \\ \hat{i}_{qmr} \end{bmatrix} + \frac{1}{\hat{\tau}_r} \begin{bmatrix} i_{ds} \\ i_{qs} \end{bmatrix} \quad (28)$$

The adaptive mechanism for rotor time constant  $\hat{\tau}_r$  can be derived from Popov's criterion for hyperstability [10] as follows

$$\frac{1}{\hat{\tau}_r} = K_1 \varphi(\varepsilon) + K_p \int \varphi(\varepsilon) dt \quad (29)$$

where  $\phi(\varepsilon)$  is the input to adaptive mechanism

$$\begin{aligned} \varphi(\varepsilon) &= (i_{dmr} - \hat{i}_{dmr})(i_{ds} - \hat{i}_{dmr}) + (i_{qmr} - \hat{i}_{qmr}) \\ &\quad \times (i_{qs} - \hat{i}_{qmr}) \end{aligned} \quad (30)$$

To use multi-rate control, the MRAS model needs to be discretised; here the trapezoidal rule is utilised for discretisation. Using derived discretised MRAS equations and motor equations as the control object, we combine input multi-rate control with discretised MRAS estimation method from (27) and (28). The sampling period of output vector is  $T_o$  and the sampling period of input vector is  $T_i$ , where  $T_o = NT_i$ ,  $N = 1, 2, \dots$ . Similar to input multi-rate EKF algorithm, we define the input extended vector and extended coefficient matrices as

$$\mathbf{u}_i(k)(2N \times 1) = [\mathbf{u}(k) \quad \mathbf{u}(k+1) \quad \dots \quad \mathbf{u}(k+N-1)]^T \quad (31)$$

$$\mathbf{B}_i(6 \times 2N) = [A^{N-1}\mathbf{B} \quad A^{N-2}\mathbf{B} \quad \dots \quad \mathbf{B}] \quad (32)$$

Using the extended vectors, the first equation in the reference model (27) is transformed as

$$\begin{aligned} \frac{d}{dx} i_{dmr} &= \frac{L_r}{L_m^2} (v_{ds}) - \left( r_s i_{ds} + \sigma L_s \frac{di_{ds}}{dx} \right) \\ &= \frac{L_r}{L_m^2} \begin{bmatrix} v_{ds}(kT_o) \\ v_{ds}(kT_o + T_i) \\ \vdots \\ v_{ds}(kT_o + (N-1)T_i) \end{bmatrix} \\ &\quad - \begin{bmatrix} r_s \begin{bmatrix} i_{ds}(kT_o) \\ i_{ds}(kT_o + T_i) \\ \vdots \\ i_{ds}(kT_o + (N-1)T_i) \end{bmatrix} \\ + \sigma L_s \frac{d}{dx} \begin{bmatrix} i_{ds}(kT_o) \\ i_{ds}(kT_o + T_i) \\ \vdots \\ i_{ds}(kT_o + (N-1)T_i) \end{bmatrix} \end{bmatrix} \end{aligned} \quad (33)$$

Similarly, the other extended equations can be obtained.

As shown in Fig. 4, at time points  $KT_o$ ,  $KT_o + T_i$ ,  $KT_o + 2T_i$  and  $KT_o + 3T_i$ , the input voltage and current are sampled; flux and current will be iteratively estimated from discretised MRAS equation and motor equation. At the beginning of next time period  $(K+1)T_o$ , the estimated  $i_{mr}$  is sent to MRAS module to estimate rotor time constant.

### 3 Experimental results and comparison

To validate the proposed multi-rate estimation algorithms, an experimental set-up shown in Fig. 5 was proposed. The LabVolt® 0.25 HP squirrel cage induction motor was used in this set-up whose parameters are given in Table 2 in the appendix. This motor was coupled to a 0.25 HP dynamometer for loading and measuring the speed and the torque. The coupled LabVolt® motor provided the

measurement interface to measure the machine voltages. The analog signals are collected by the sensors and patch panel and converted to  $\pm 10$  V range. These signals are then sampled by the A/D cards in the real-time simulator which uses the RT-LAB environment [27]. The multi-rate parameter estimation methods proposed in this paper are implemented in real-time as dynamically linked *s*-function's in the MATLAB/Simulink environment. The algorithms are compiled using real-time workshop and downloaded to the real-time simulator for execution. The experimental and estimated signals can be viewed in real-time on the host-PC, which is connected to the real-time simulator through gigabit ethernet.

The input multi-rate EKF algorithm is applied in the open-loop experiment. Fig. 6 shows the experimental result; the proposed algorithm gives satisfied estimated speed which match the actual speed smooth even when the torque changes. Fig. 7 shows the simulation of close-loop field-oriented controlled induction motor with multi-rate EKF estimator. The inputs of the estimator are voltages and currents obtained from the induction motor; the outputs contain the estimated load torque and speed. The sampling period for controlling the speed and the current components is  $16e-5s$ . The single-rate EKF load torque estimate result is shown in Fig. 8a with a system sampling period of  $T_s = 16e-5s$ . The reference speed is set to 100 rad/s, which is 57% of the rated speed. The result shows that single-rate EKF load torque observation effect is good, but stability is not satisfied, as the noise will detune the performance of system. The design of the input multi-rate EKF load torque observation algorithm is based on the proposed recurrence formula. In this algorithm, the output sampling period is  $T_o = 16e-5s$ , input sampling period is  $T_i = 4e-5s$ ,  $T_i = 2e-5s$ , the sampling multiplicity being  $N=4$ , and  $N=8$ , respectively. The input sampling period is a fraction of the output sampling period, however, the frame period is still  $16e-5s$ , which equals the single-rate frame period. The values of covariance matrix elements influence the filter performance.  $\mathbf{Q}$  and  $\mathbf{R}$  are covariance matrices of process and observation noise, respectively, which are chosen in diagonal form to alleviate computational complexity. For the proposed model:  $\mathbf{P} = [50A^2 \ 50A^2 \ 0.01 \ (V \cdot s)^2 \ 0.01 \ (V \cdot s)^2 \ 20 \ (rad/s)^2 \ 5 \ (N \cdot m)^2]$ ;  $\mathbf{Q} = [50A^2 \ 50A^2 \ 0.01 \ (V \cdot s)^2 \ 0.01 \ (V \cdot s)^2 \ 20 \ (rad/s)^2 \ 5 \ (N \cdot m)^2]$ ;  $\mathbf{R} = [50A^2 \ 50A^2]$ . Figs. 8b and c show the input multi-rate EKF load torque estimation results. Comparing with single-rate EKF result reveals that the input multi-rate EKF improved the load torque estimate effect significantly. Input multi-rate EKF reduced the estimate error effectively, improved the observation accuracy and reduced the system stability time.

With an increase in sampling multiplicity, the observation improves. The reason is that with the increase of effective input number, the control ability of the controller improves. From the perspective of continuous-time, the single-rate control system can only realise the feedback at the sampling points; however, during other times in the sampling period the system is open-loop. Depending on the control objective, multi-rate control can realise feedback control at other points in the sampling period, thus improving the controller performance. The output multi-rate EKF load torque observation algorithm was designed based on the recurrence formula with input sampling period  $T_i = 16e-5s$ , and output sampling periods  $T_o = 4e-5s$ ,  $T_o = 2e-5s$ , the sampling multiplicity being  $N=4$ , and  $N=8$ , respectively. Figs. 8e and f are the output multi-rate EKF load torque estimate simulation results. In comparison with



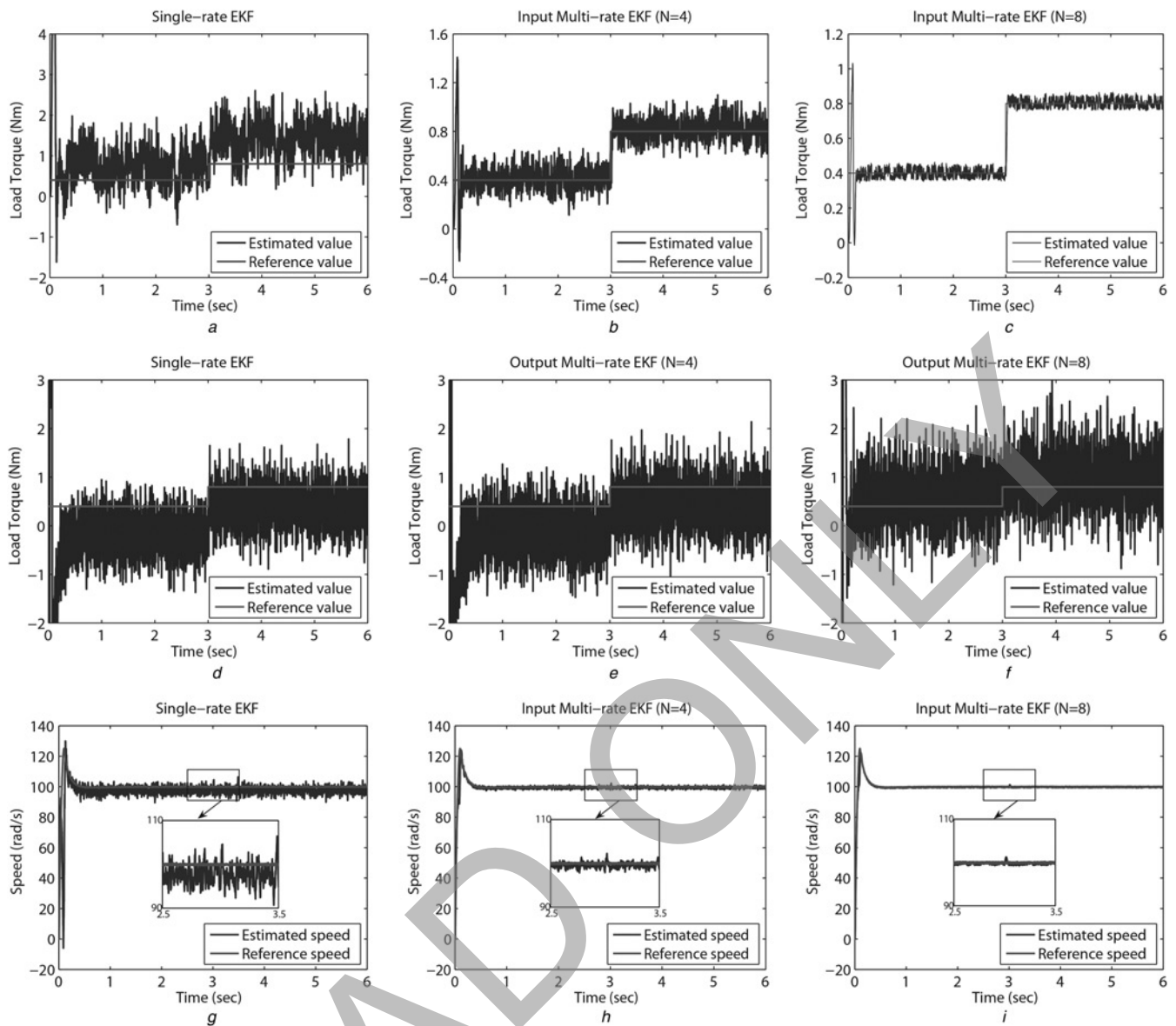


**Fig. 8** Comparison of load torque estimation

a–c By single-rate EKF and input multi-rate EKF  
 d–f By single-rate EKF and output multi-rate EKF  
 g–i By single-rate EKF and input multi-rate EKF

16e–5s) with single-rate EKF (sampling period: 4e–5s), the execution time of both methods is 134s. the complexity and the observation performance is almost the same; however, the output sampling frequency of the former is much lower, which means multi-rate EKF reduced the hardware requirement. From this perspective, the multi-rate EKF lowers the cost of system without lowering the system performance.

**Table 1** Performance comparison of input and output multi-rate EKF with single-rate EKF

| Algorithm                     | Relative error | Variance |
|-------------------------------|----------------|----------|
| single-rate EKF               | 0.2365         | 0.1045   |
| input multi-rate EKF $N = 4$  | 0.0248         | 0.0068   |
| input multi-rate EKF $N = 8$  | 0.0075         | 0.0006   |
| output multi-rate EKF $N = 4$ | 0.2302         | 0.1395   |
| output multi-rate EKF $N = 8$ | 0.0822         | 0.2094   |

Figs. 8g–i show the comparison of the speed estimation result. With the increase of sampling multiplicity  $N$ , the estimation accuracy improves significantly not only because of the increase of sampling multiplicity but also because of the advantages of multi-rate algorithm. The precise speed

**Table 2** System variables and parameters

| Parameter                      | Value                        |
|--------------------------------|------------------------------|
| output power                   | 175 W                        |
| moment of inertia              | 0.0022 kg m <sup>2</sup>     |
| $R_r, R_s$                     | 8 Ω, 12 Ω                    |
| $L_r, L_s, L_m$                | 48.3e–2H, 48.3e–2H, 45.4e–2H |
| number of pole pairs ( $n_p$ ) | 2                            |
| full load speed                | 1670 rpm                     |
| full load current              | 1.2 A                        |
| phase voltage                  | 120 V                        |
| frequency                      | 60 Hz                        |
| (1/τ <sub>r</sub> )            | 16.56 (1/s)                  |

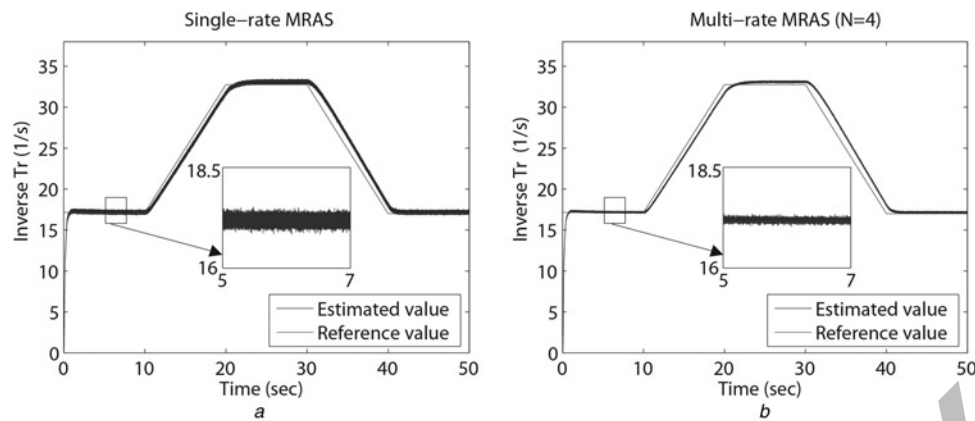


Fig. 10 Comparison of rotor time constant estimation by single-rate MRAS and input multi-rate MRAS

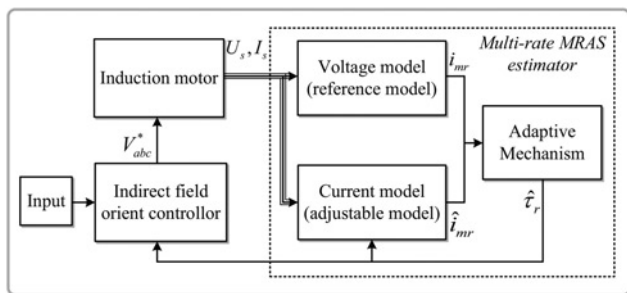


Fig. 9 Simulation of IM with MRAS estimator

and load torque estimation guarantee the high performance of the AC drive; however, with the increase of sampling multiplicity  $N$ , the computation burden also increases. Although the current processing power is enough for the extra computation, in practice, choosing appropriate sampling multiplicity to balance the control ability and calculation burden is recommended.

Fig. 9 shows the simulation structure of the multi-rate MRAS method. Reference inverse rotor time constant uses a varying ramp function to emulate practical situations. The PI controller gain  $K_P$ ,  $K_I$  in (29) are set as  $K_P = 0.01382$  and  $K_I = 370$ . The gains were tuned according to experience and experiment performance. The results of MRAS estimation under constant speed operation are shown in Fig. 10. The input multi-rate MRAS estimation simulation was designed with output sampling period  $T_o = 16e - 5s$  and input sampling period  $T_i = 4e - 5s$ . The frame period of input multi-rate MRAS algorithm is  $16e - 5s$  as the single-rate's frame period. Figs. 10a and b show the single-rate MRAS and input multi-rate MRAS estimation result, respectively. A comparison shows that the proposed multi-rate MRAS algorithm improved rotor time constant estimation accuracy. Variance of the single-rate result is 0.0070, whereas the variance of the multi-rate result is only 0.0018. The result indicates that the multi-rate MRAS method improved system stability efficiently.

## 4 Conclusion

This paper proposed multi-rate real-time model-based methods for parameter and state estimation of induction motor. A multi-rate EKF load torque estimation algorithm is proposed; both input and output algorithms are introduced. This method is applied to the motor FOC

system, the method is implemented in real-time on a PC cluster node that acts as a controller to an induction motor experimental set-up. Experimental results verified the effectiveness of the algorithm. The comparison result shows that the multi-rate control scheme efficiently improved the accuracy of load torque estimation. Estimated load torque follows the reference load torque closely and with better noise immunity compared with single-rate EKF. This novel multi-rate method improves traditional EKF method and brings many advantages to motor parameter estimation. Rotor time constant is the most sensitive parameter in indirect FOC. This paper proposed a novel method to estimate the rotor time constant. The proposed method use multi-rate control strategy to estimate flux; the obtained flux is then imported into the MRAS scheme, where the magnetising current is used as comparison quantity from reference and adjustable model. The result verified that the proposed multi-rate MRAS method is efficient and reliable.

## 5 Acknowledgment

This work was supported by the National Natural Science Foundation of China (51177137 and 61134001) and China CNR Corporation Limited. The authors would like to thank the anonymous reviewers for their constructive and useful comments/suggestions which helped us to improve the quality and readability of the manuscript.

## 6 References

- 1 Toliyat, H.A., Levi, E., Raina, M.: 'A review of RFO induction motor parameter estimation techniques', *IEEE Trans. Energy Convers.*, 2003, **18**, (2), pp. 271–283
- 2 Barut, M., Bogosyan, S., Gokasan, M.: 'Speed-sensorless estimation for induction motors using extended kalman filters', *IEEE Trans. Ind. Electron.*, 2007, **54**, (1), pp. 272–280
- 3 Holtz, J.: 'Sensorless control of induction machines – with or without signal injection?', *IEEE Trans. Ind. Electron.*, 2006, **53**, (1), pp. 7–30
- 4 Holtz, J., Quan, J.: 'Drift- and parameter-compensated flux estimator for persistent zero-stator-frequency operation of sensorless-controlled induction motors', *IEEE Trans. Ind. Appl.*, 2003, **39**, (4), pp. 1052–1060
- 5 Gao, Z., Habetler, T.G., Harley, R.G., Colby, R.S.: 'A sensorless rotor temperature estimator for induction machines based on a current harmonic spectral estimation scheme', *IEEE Trans. Ind. Electron.*, 2008, **55**, (1), pp. 407–416
- 6 Pedra, J., Sainz, L.: 'Parameter estimation of squirrel-cage induction motors without torque measurements', *IEE Proc. Electr. Power Appl.*, 2006, **153**, (2), pp. 263–270
- 7 Blasco-Giménez, R., Asher, G.M., Sumner, M., Bradley, K.J.: 'Dynamic performance limitations for MRAS based sensorless induction motor drives – Part 1: stability analysis for the closed loop drive', *IEE Proc. Electr. Power Appl.*, 1996, **143**, (2), pp. 113–122

- 8 Pea, R., Cerdas, R., Proboste, J., Asher, G., Clare, J.: 'Sensorless control of doubly-fed induction generators using a rotor-current-based MRAS observer', *IEEE Trans. Ind. Electron.*, 2008, **55**, (1), pp. 330–339
- 9 Garcia Soto, G., Mendes, E., Razek, A.: 'Reduced-order observers for rotor flux, rotor resistance and speed estimation for vector controlled induction motor drives using the extended Kalman filter technique', *IEE Proc. Electr. Power Appl.*, 1999, **146**, (3), pp. 282–288
- 10 Zaky, M.S., Khater, M.M., Shokralla, S.S., Yasin, H.A.: 'Wide-speed-range estimation with online parameter identification schemes of sensorless induction motor drives', *IEEE Trans. Ind. Electron.*, 2009, **56**, (5), pp. 1699–1707
- 11 Yang, I.-W., Kim, Y.-S.: 'Rotor speed and position sensorless control of a switched reluctance motor using the binary observer', *IEE Proc. Electr. Power Appl.*, 2000, **147**, (3), pp. 220–226
- 12 Barut, M., Bogosyan, S., Gokasan, M.: 'Experimental evaluation of braided EKF for sensorless control of induction motors', *IEEE Trans. Ind. Electron.*, 2008, **55**, (2), pp. 620–632
- 13 Zarchi, H.A., Soltani, J., Markadeh, G.A.: 'Adaptive input-output feedback-linearization-based torque control of synchronous reluctance motor without mechanical sensor', *IEEE Trans. Ind. Electron.*, 2010, **57**, (1), pp. 375–384
- 14 Huynh, D.C., Dunnigan, M.W.: 'Parameter estimation of an induction machine using advanced particle swarm optimisation algorithms', *IET Electr. Power Appl.*, 2010, **4**, (9), pp. 748–760
- 15 Monmasson, E., Idkhajine, L., Cirstea, M.N., Bahri, I., Tisan, A., Naouar, M.W.: 'FPGAs in industrial control applications', *IEEE Trans. Ind. Inf.*, 2011, **7**, (2), pp. 224–243
- 16 Kranc, G.: 'Input-output analysis of multirate feedback systems', *IEEE Trans. Autom. Control*, 1957, **3**, (1), pp. 21–28
- 17 Patton, R.J., Lui, G.P., Patel, Y.: 'Sensitivity properties of multirate feedback control systems, based on eigenstructure assignment', *IEEE Trans. Autom. Control*, 1995, **40**, (2), pp. 337–342
- 18 Yamamoto, Y.: 'A function space approach to sampled data control systems and tracking problems', *IEEE Trans. Autom. Control*, 1994, **39**, (4), pp. 703–713
- 19 Xiao, J., Tang, L.: 'Pole assignment of multirate digital control systems with decentralized structure'. Proc. 2000 Int. Workshop on Autonomous Decentralized Systems, Chengdu, China, September 2000, pp. 216–221
- 20 Qiu, L., Chen, T.: ' $H_2$ -optimal design of multirate sampled-data systems', *IEEE Trans. Autom. Control*, 1994, **39**, (12), pp. 2506–2511
- 21 Sagfors, M.F., Toivonen, H.T., Lennartson, B.: 'State-space solution to the periodic multirate  $H_\infty$  control problem: a lifting approach', *IEEE Trans. Autom. Control*, 2000, **45**, (12), pp. 2345–2350
- 22 Sheng, J., Chen, T., Shah, S.L.: 'Optimal filtering for multirate systems', *IEEE Trans. Circuits Syst. II, Express Briefs*, 2005, **52**, (4), pp. 228–232
- 23 Saiki, K., Hara, A., Sakata, K., Fujimoto, H.: 'A study on high-speed and high-precision tracking control of large-scale stage using perfect tracking control method based on multirate feedforward control', *IEEE Trans. Ind. Electron.*, 2010, **57**, (4), pp. 1393–1400
- 24 Yamaguchi, N., Hasegawa, M., Doki, S., Okuma, S.: 'New approach for stability improvement of speed sensorless induction-motor controls at zero frequency using multirate adaptive observer', *IEE Proc. Electr. Power Appl.*, 2006, **153**, (4), pp. 544–550
- 25 Tajima, H., Hori, Y.: 'Speed sensorless field-orientation control of the induction machine', *IEEE Trans. Ind. Appl.*, 1993, **29**, (1), pp. 175–180
- 26 Chui, C.K., Chen, G.: 'Kalman filtering: with real-time application' (Springer, Berlin, 2009, 3rd edn.)
- 27 'RT-LAB 8 user manual' (Opal-RT Technology Inc., Montreal, QC, Canada, 2006), pp. 1–80

## 6 Appendix 1

Table 2 shows the system parameters.